Shape model and Hermite features for the segmentation of the cerebellum in fetal ultrasound

Reyes López, Misael, Arámbula Cosío, Fernando , Escalante-Ramírez, Boris, Olveres, Jimena

Misael Reyes López, Fernando Arámbula Cosío, Boris Escalante-Ramírez, Jimena Olveres, "Shape model and Hermite features for the segmentation of the cerebellum in fetal ultrasound," Proc. SPIE 10975, 14th International Symposium on Medical Information Processing and Analysis, 1097514 (21 December 2018); doi: 10.1117/12.2511411

SPIE.

Event: 14th International Symposium on Medical Information Processing and Analysis, 2018, Mazatlán, Mexico

Shape model and Hermite features for the segmentation of the cerebellum in fetal ultrasound

Misael Reyes López[a], Fernando Arámbula Cosío[b], Boris Escalante-Ramírez[c], Jimena Olveres[c]
[a]Posgrado en Ciencia e Ingeniería de la Computación,
[b]Instituto de Investigaciones en Matemáticas Aplicadas y en Sistemas,
[c]Deparatamento de Procesamiento de Señeales, Facultad de Ingeniería,
Universidad Nacional Autónoma de México (UNAM), Mexico City, 04510

ABSTRACT

In this paper we propose a semi-automatic method to segment the fetal cerebellum in ultrasound images. The method is based on an active shape model which includes profiles of Hermite features. In order to fit the shape model we used a PCA of Hermite features. This model was tested on ultrasound images of the fetal brain taken from 20 pregnant women with gestational weeks varying from 18 to 24. Segmentation results compared to manual annotation show a mean Hausdorff distance of 6.85 mm using a conventional active shape model trained with gray profiles, and a mean Hausdorff distance of 5.67 mm using Hermite profiles. We conclude that the Hermite profile model is more robust in segmenting fetal cerebellum in ultrasound images.

Keywords Segmentation, ultrasound, active shape model, Hermite transform, fetal cerebellum

1. INTRODUCTION

Ultrasound images are used frequently for the morphological and biometric analysis of fetal brain structures (ventricular atrium, cerebellum, cisterna magna, etc.) for purposes of evaluation of the fetal development [1] [2], but sometimes manual segmentation of these structures is very time consuming for studies which have a large amount of data. This is a reason to develop automatic methods that help in segmentation tasks. However, the automatic or semi-automatic segmentation in ultrasound images is challenging because the image quality is substantially degraded by the speckle patterns [3], [4], [5], [6], [7] [8]. An approach that has been widely used to improve the segmentation in ultrasound images is based in the use statistical shape models. These models have gained great popularity because they incorporate expert shape knowledge from annotations on the image data. A particular case of statistical shape model is the active shape model [9]. These models have demonstrated that the resulting segmentation improves with the integration of *a priori* information of shape and appearance (grey level models) in the training set. On the other hand, the image texture is valuable information used among other things in the segmentation tasks and in this respect, the Hermite transform have demonstrated be able to detect image texture and in this study our PCA model has been able to detect organ boundaries based on textures edges. In this paper, we report an active shape model that uses an image texture model based on the steered Hermite transform for the improved automatic segmentation of the fetal cerebellum, as reported in the following sections.

2. ACTIVE SHAPE MODEL (ASM)

In an ASM, the shape knowledge of the object is integrated within a compact form using a statistical model trained with examples [9] [10]. This model contains the information of mean shape and its variations thus ensuring that the resulting segmentation is a coherent shape with respect to the training set.

Each example in the training set is stored in a $2n$ shape vector $\boldsymbol{x} = (x_1, y_1, \dots, x_n, y_n)^T$. After, all examples are translated, scaled and rotated in order to align them. The mean shape is computed as

14th International Symposium on Medical Information Processing and Analysis,
edited by Eduardo Romero, Natasha Lepore, Jorge Brieva, Proc. of SPIE Vol. 10975,
1097514 · © 2018 SPIE · CCC code: 0277-786X/18/$18 · doi: 10.1117/12.2511411

$$\bar{\boldsymbol{x}} = \frac{1}{N}\sum_{i=1}^{N} \boldsymbol{x_i} \tag{1}$$

where N is the number of examples.

For each example in the training set we calculate its deviation from the mean, $d\boldsymbol{x_i}$, where

$$\boldsymbol{dx_i} = \boldsymbol{x_i} - \bar{\boldsymbol{x}} \tag{2}$$

Considering the deviation, we compute the $2n \times 2n$ covariance matrix, $\boldsymbol{S}$, using

$$\boldsymbol{S} = \frac{1}{N}\sum_{i=1}^{N} d\boldsymbol{x}_i d\boldsymbol{x}_i^T \tag{3}$$

With the covariance matrix, we obtain the modes of variation of the points of the shape that will allow us to approximate new shapes $\boldsymbol{x}$ of the model

$$\boldsymbol{x} = \bar{\boldsymbol{x}} + \boldsymbol{P_s b_s} \tag{4}$$

where $\bar{\boldsymbol{x}}$ is the mean shape, $\boldsymbol{P_s} = (\boldsymbol{p_1}\, \boldsymbol{p_2} \ldots \boldsymbol{p_t})$ contains the t eigenvectors of the covariance matrix and $\boldsymbol{b_s} = (b_1\ b_2 \ldots b_t)^T$ is a vector of weights of the shape representation. The variation of the i^{th} parameter, b_i, is defined by the eigenvalues λ_i. These variations are limited to $b_i = \pm 3\sqrt{\lambda_i}$ to ensure that the generated shapes are similar to those of the training set.

We build a Point Distribution Model (PDM) of the cerebellum and we use the principal modes of variation that comprise at least 90% of the shape information. In figure 1 we show examples of the fetal cerebellum with its respective manual annotation and some modes of variation of the cerebellum.

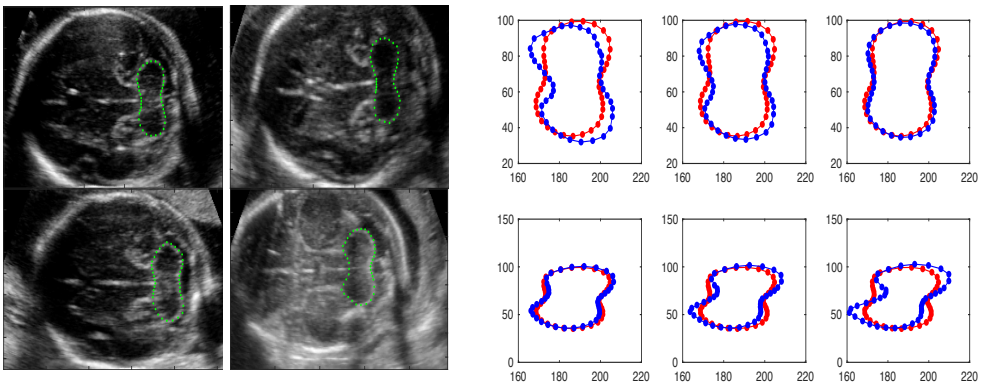

Figure 1. Training set images. a) Example shapes of a fetal cerebellum; b) Six modes of shape variation from training set in blue points and the mean shape in red points.

For the adjustment stage is necessary to sample gray level profiles which are normal to each landmark in the object, afterwards these profiles are stored to create a training set of gray levels. In figure 2 we can see an example of gray profiles acquired from a fetal cerebellum ultrasound image.

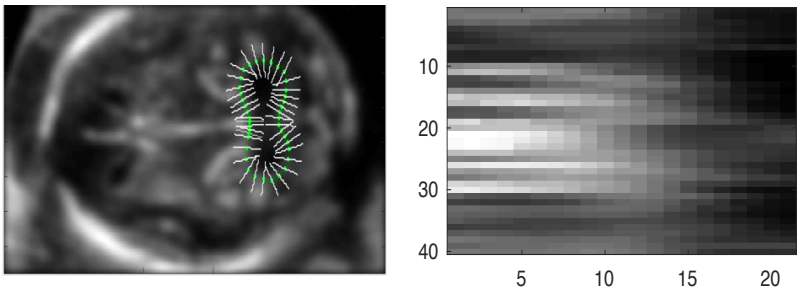

a) b)

Figure 2. Acquisition of gray profile. a) Normal profile in each landmark. b) Gray level profiles. Each row is a gray level profile and correspond to each landmark of the cerebellum.

We can observe that the cerebellum is a structure with a semi-defined shape (see figures 1 and 2).

Finally, in order to fit the ASM within the set of landmarks, gray level profiles are compared with their respective training gray level profiles until the minimal error is found.

3. HERMITE TRANSFORM

The Hermite transform (HT) belongs to the family of polynomial transforms and is used because it incorporates Gaussian derivatives as basis functions which resemble the response of receptive fields of the human visual system in its first stages [11] [12] [13] [14]. The below equation shows the definition of these functions:

$$D_n(x) = \frac{(-1)^n}{\sqrt{2^n n!}} \frac{1}{\sigma\sqrt{\pi}} H_n\left(\frac{x}{\sigma}\right) \exp\left(\frac{-x^2}{\sigma^2}\right) \tag{5}$$

where n indicates the order of the polynomial and σ the spread of the Gaussian window.

The resulting Hermite functions satisfy the property of separability, so the 2D model is straight forward defined as $D_{n-m,m}(x,y) = D_{n-m}(x)D_m(y)$. The HT expands the input 2D signal into a set of polynomial coefficients that represent a description of relevant information such as edges, lines, textures, etc.

The discrete implementation is obtained by convolving the input image with the set of Hermite analysis filters defined by

$$L_{n-m,m}(x_0, y_0) = \iint_{-\infty}^{\infty} I(x,y) D_{n-m,m}(x_0 - x, y_0 - y)\,dx\,dy, \tag{6}$$

for $n = 0,1, \dots, \infty$ and $m = 0, \dots, n$. This definition is known as the Cartesian HT.

Another representation of the HT is the steered Hermite transform (SHT). The steering property is useful to adapt local orientation content according to a criterion of maximum oriented energy, then achieving compaction [4]. The next equations show hot to obtain the SHT:

$$L^{\theta}_{n-m,m}(x_0, y_0) = \sum_{k=0}^{n} L_{n-k,k}(x_0, y_0) R_{n-k,k}(\theta), \tag{7}$$

$$R_{n-m,m}(\theta) = \sqrt{\binom{m}{n}} \cos^{n-m}\theta \sin^{m}\theta, \tag{8}$$

where $R_{n-m,m}(\theta)$ are known as the cartesian angular functions, which indicate the direction of maximum oriented energy at all window positions.
The SHT has been previously used on applications, such as, medical organ segmentation and texture analysis offering good results [15] [16] [17] [18] [19] [20].

In the figure 3 we show up to second order of the steered Hermite coefficients of the fetal cerebellum.

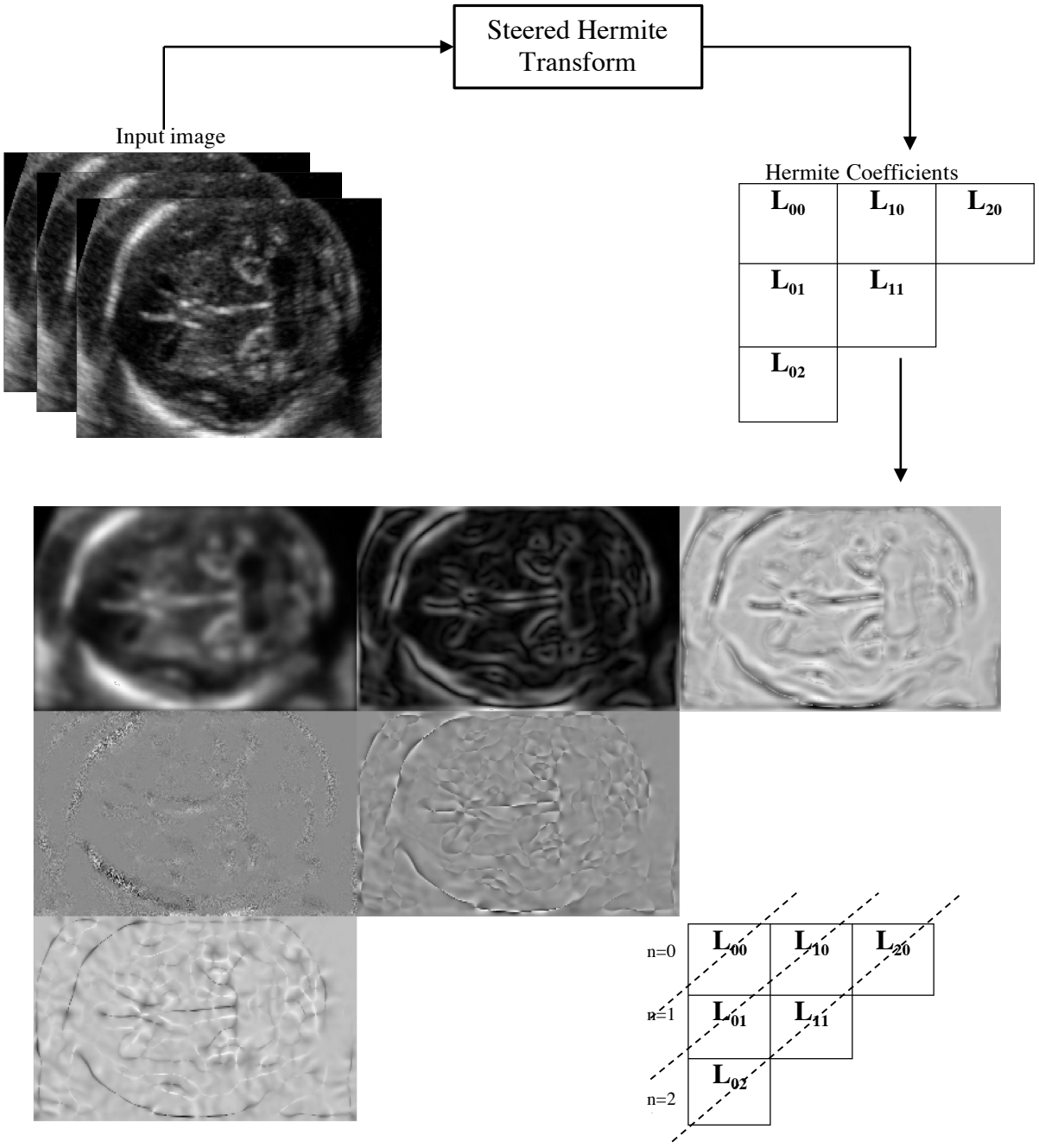

Figure 3. Coefficients up to second order of the steered Hermite transform using a fetal cerebellum image

4. PROPOSED METHOD

Our method is a variation of the original ASM; the idea that we propose is basically to use Hermite feature profiles instead of gray level profiles. Furthermore, in order to fit the ASM to the training data, we use a Principal Component Analysis (PCA) of the Hermite features instead of the mean gray. The steps of the proposed method are described below.

First, we build the PDM of the cerebellum as we explained in section 2. Then we obtain the steered Hermite coefficients up to second order of the training images (see figure 3) and for our case only we use the first three coefficients (L_{00}, L_{10} and L_{20}) to build the Hermite feature profiles. In figure 4 we present a scheme of the construction of these profiles.

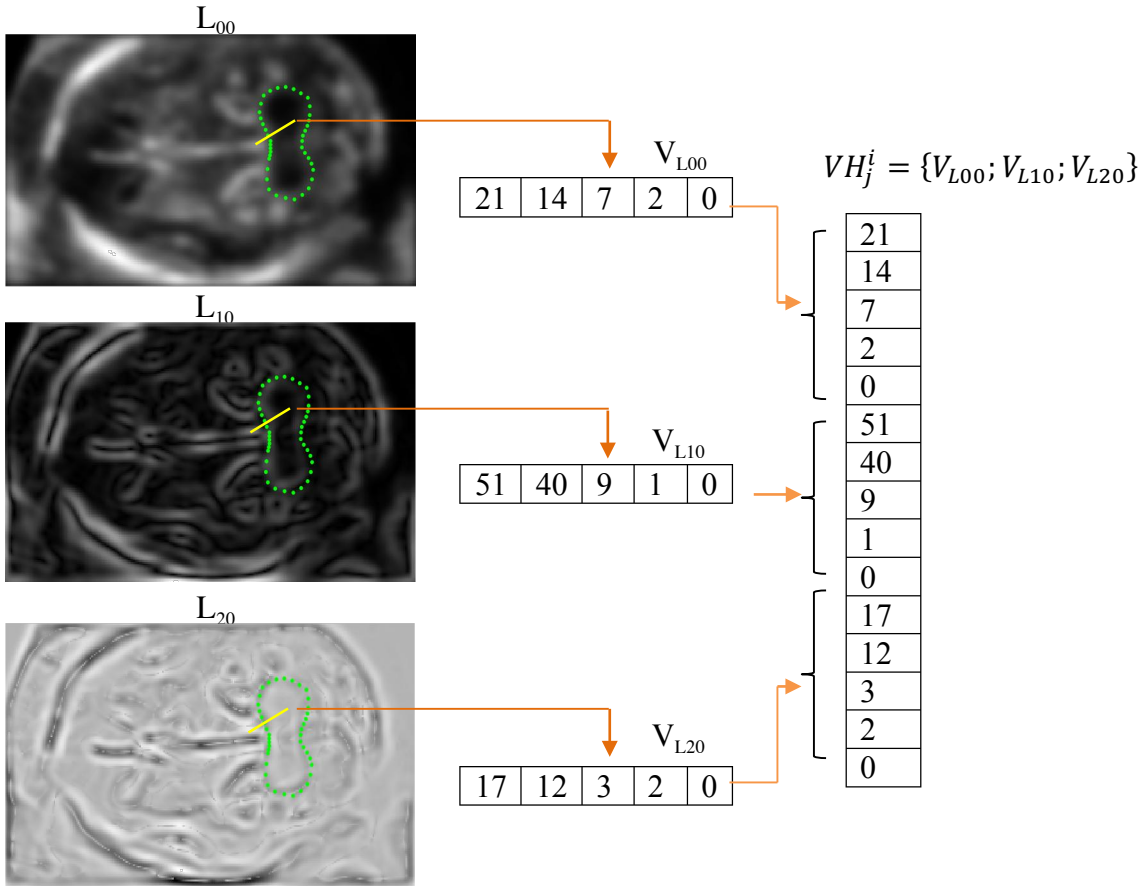

Figure 4. Building of the Hermite's vector VH for the point i in the image j.

In figure 4 we show the construction of the Hermite vector $VH_j^i = \{V_{L00}; V_{L10}; V_{L20}\}$ by concatenation of the data of the profiles of the Hermite coefficients for point i, where V_{L00}, V_{L10} and V_{L20} are the Hermite feature profiles acquired of the steered Hermite coefficients L_{00}, L_{10} and L_{20} respectively, $j = 1 \ldots n$ is the image number of the training set and $i = 1 \ldots N$ is the point number of the shape model of the cerebellum. If the previous process is repeated for the same point i in all images of the training set we will obtain their corresponding Hermite vectors $VH_1^i, VH_2^i, \ldots, VH_n^i$ (see figure 5).

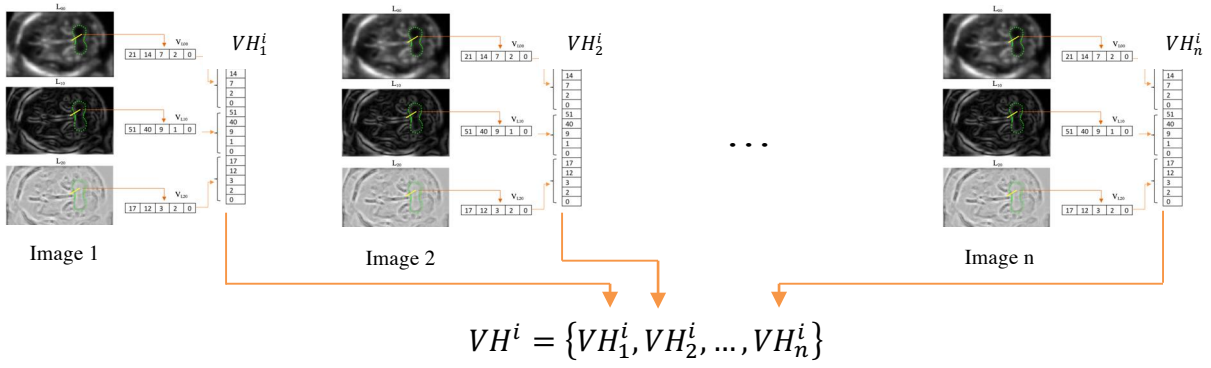

Figure 5. Construction of the Hermite vector VH^i for the point *i* considering all images of the training set.

With the information contained in VH^i is possible to compute the Hermite feature mean $\mu(VH^i)$ and the covariance matrix $\sum(VH^i)$ in the point *i*, as well as its corresponding PCA.

If the process presented in figures 4 and 5 is applied to each landmark (1…*N*) of the cerebellum model we obtain a PCA for each of them. Finally, using the PCA information in each landmark we propose the next fitting function:

$$f_{obj} = PT_{PCA}^i - PT_{analized}^i \tag{9}$$

where PT_{PCA}^i is the Hermite profile obtained from PCA and $PT_{analized}^i$ is the Hermite profile obtained from the input image in the point *i*.

5. TESTS AND RESULTS

The proposal was evaluated on 20 different ultrasound images taken of 20 different ultrasound volumes acquired in an axial plane by a Voluson 730 Expert from General Electric. The volumes were obtained with informed consent of patients at the National Institute of Perinatology in Mexico City. An expert perinatologist realized the manual annotation of the cerebellum.

Both the original ASM and our proposed ASM was evaluated on the training set using the leave-one-out methodology. 19 images were used for training with validation on the image that was left out. This process was repeated 20 times. The Hausdorff distance was used to measure the accuracy of the semi-automatic segmentation of the both methods against manual expert annotations.

In the original ASM we used smoothed images to reduce the speckle pattern present in the images. We used a Gaussian filter with standard deviation (σ) equal to 2.

For both methods (original ASM and proposed ASM) the segmentation was performed on the full image size, with the same initialization (mean shape of the cerebellum located in the center of the structure), and the adjustment process was limited to 40 iterations. The results are shown in table 1.

Table 1. Segmentation results

Segmented image	Hausdorff distance (original ASM) [mm]	Hausdorff distance (proposed ASM) [mm]
1	6.17	3.84
2	5.08	5.10
3	8.57	6.38
4	10.02	9.16
5	9.05	7.03

6	6.02	8.86
7	7.23	5.62
8	4.98	4.60
9	8.20	5.33
10	7.67	3.90
11	5.54	5.40
12	8.63	6.00
13	5.23	5.51
14	4.46	4.37
15	4.50	5.71
16	6.53	3.93
17	6.47	4.45
18	5.85	4.99
19	8.86	6.71
20	7.87	6.51
Mean	**6.85**	**5.67**
Standard deviation	**1.67**	**1.47**

In figure 6 we show the three best results (image 1, image 10 and image 16) and the worst result (image 4) for the proposed ASM.

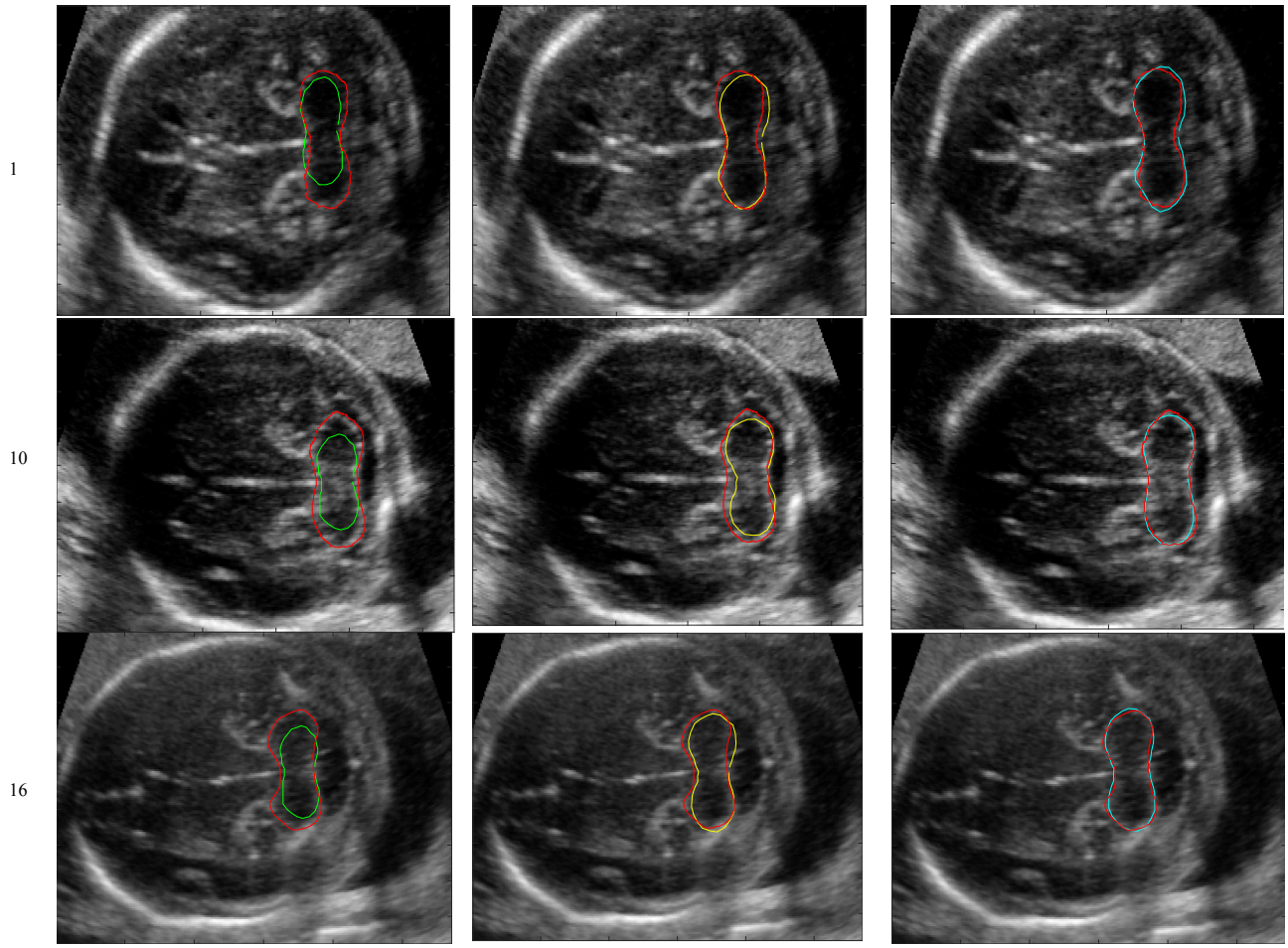

4

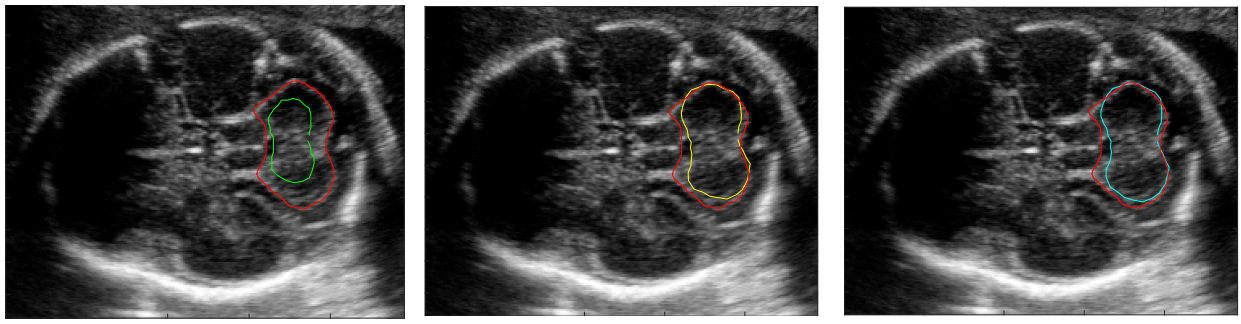

a. b. c.

Figure 6. Results of a cerebellum segmentation obtained with 40 iterations. (a) Initial shape (green line) and manual annotation (red line), b) Comparison between final segmentation of the original ASM (yellow line) and manual annotation (red line), (c) Comparison between final segmentation of our proposed ASM (cyan line) and manual annotation (red line).

6. DISCUSSION AND CONCLUSIONS

As reflected in Table 1, our ASM proposed method presents good results for the segmentation of fetal cerebellum in ultrasound images. Some examples of these results are presented in the figure 6, where we can see that in the first three cases (row) the segmentation given by our method (column 3, cyan line) is very similar to the manual annotation (red line), in contrast to the results of the original ASM.
The worst result in both methods was the case of image 4, however we can observe that the result given for our method (cyan line) is closer to the cerebellum edges (upper and lower lobe) than the original ASM result.
In the fitting stage, our method was more stable than the original ASM, the reason is because the images of the Hermite coefficients presented more information of the cerebellum edges than a smoothed image with a Gaussian filter.
As consequence of the previous point, in our proposed method we observed that if the cerebellum has defined edges then there is a higher probability of correct segmentation of the cerebellum.
Considering the mean Hausdorff distance of the original ASM (6.85 mm) and the proposed ASM (5.67 mm), we conclude that our proposed ASM keeps a closer resemblance with the manual expert annotation.
We also conclude that the steered Hermite transform is an efficient ultrasound image descriptor that allows a better adjustment of the shape model to the cerebellum.

REFERENCES

[1] I. Claude, J. L. Daire y G. Sebag, «Fetal Brain MRI: Segmentation and Biometric Analysis of the Posterior Fossa,» *IEEE Transactions on Biomedical Engineering* , vol. 51, nº 4, pp. 617-626, 2004.

[2] I. Timor-Tristch, A. Monteagudo y H. Cohen, Neuroecografía Prenatal y Neonatal, Marban, 2004.

[3] F. Arámbula Cosío, «Automatic initialization of an active shape model of the prostate,» *Medical Image Analysis,* vol. 12, nº 4, pp. 469-483, 2008.

[4] B. Gutiérrez Becker y F. Arámbula Cosío , Segmentación del cerebelo de fetos en ultrasonido 3D, México: UNAM, 2011.

[5] B. Gutiérrez Becker, F. Arámbula Cosío, M. E. Guzmán Huerta, J. A. Benavides-Serralde, L. Camargo Marín y V. Médina Bañuelos, «Automatic segmentation of the fetal cerebellum on ultrasound volumes, using a 3D statitical shape model,» *Medical and Biological Engineering and Computing,* vol. 51, nº 9, pp. 1021-1030, 2013.

[6] G. Velásquez Rodríguez y F. Arámbula Cosío , Medición automática del pliegue nucal en imágenes de ultrasonido tridimensional, México: UNAM, 2013.

[7] G. Velásquez Rodríguez y F. Arámbula Cosío, «Segmentación tridimensional del cerebelo fetal mediante armónicos esféricos,» *SOMI XXIX Congreso de Instrumentación ,* Octubre 2014.

[8] C. Xu, D. L. Pham y J. L. Prince, «Image segmentation using deformable models,» de *Handbook of Medical Imaging* , SPIE Press, 2000, pp. 129-174.

[9] T. Cootes, C. Taylor, D. Cooper y J. Graham, «Active shape models-Their training and application,» *Computer Vision and Image Understanding ,* vol. 61, nº 1, pp. 38-59, 1995.

[10] T. Cootes, «Model-Based Methods in Analysis on Biomedical Images,» de *Image Processing and Analysis* , Oxford University Press, 2000, pp. 223-248.

[11] R. Y. R. L. y W. M. , «The Gaussian Derivative model for spatial-temporal vision: I. Cortical model,» *Spatial Vision ,* vol. 14, nº 3, pp. 261-319, 2001.

[12] J. B. Martens, «The Hermite Transform-Theory,» *IEEE Transactions on Acoustics, Speech and Signal Procesing ,* vol. 38, nº 9, pp. 1595-1606, 1990.

[13] J. B. M. «The Hermite Transform-Applications,» *IEEE Transactions on Acoustics, Speech, and Signal Processing ,* vol. 38, nº 9, pp. 1607-1618, 1990.

[14] A. M. v. D. «Image representation and compression with steered Hermite transform,» *Signal Processing ,* vol. 56, nº 1, pp. 1-16, 1997.

[15] J. O. E. C. Degante, B. E. Ramirez, E. V. y C. M. G. Moreno, «Deformable models for segmentation based on local analysis,» *Mathematical Problems in Engineering ,* 2017.

[16] L. B. Jimenez, B. E. Ramirez, E. V. Venegas y F. A. Cosio, «A 3D Hermite-based multiscale local active contour method with elliptical shape constraints for segmentation of cardiac MR and CT volumes,» *Medical & Biological Engineering & Computing ,* vol. 56, pp. 833-851, 2017.

[17] L. V. Quintero, B. E. Ramirez, L. C. Marin, M. G. Huerta, F. A. Cosio y H. B. Olivares, «Left ventricle segmentation in fetal echocardiography using a multi-texture active appearance model

based on the steered Hermite transform,» *Computer Methods and Programs in Biomedicine* , vol. 137, pp. 231-245, 2016.

[18] A. E. Romero y B. E. Ramirez, «Rotation-invariant texture features from the steered Hermite transform,» *Pattern Recognition Letters* , vol. 32, pp. 2150-2162, 2011.

[19] C. J. R. Moreno y S. B. , «Texture feature extraction and indexing by Hermite filters,» *Proceedings of 17th International Conference on Pattern Recognition* , 2004.

[20] J. Olveres, B. Escalante, E. V. y J. K. , «Left ventricle Hermite-based segmentation,» vol. 87, pp. 236-249, 2017.